SUPPORTING INFORMATION

Bottom-up Multiscale Approach to Estimate Viscoelastic Properties of Entangled Polymer Melts with High Glass Transition Temperature

Heyi Liang[†§], Kenji Yoshimoto*[‡§], Phwey Gil[†§], Masahiro Kitabata[‡], Umi Yamamoto[‡], Juan J. de Pablo*[†]

[†]Pritzker School of Molecular Engineering, The University of Chicago, Chicago, Illinois 60637, United States.

[‡]Toray Industries Inc., 3-2-1 Sonoyama, Otsu, Shiga 520-0842, Japan.

S.1 Simulation Details

S.1.1 All-Atom (AA) Simulations

We performed AA simulations using GROMACS 5.1.4 software[1-3]. The potential formulae and parameters (including charges) were determined from the standard OPLS-AA force field[4], and the molecular topology file was generated by free software, MKTOP[5]. The time step for the molecular dynamics simulations was set to 1 fs. To facilitate the computational speed, the bond lengths between the hydrogen and carbon atoms were constrained with LINCS algorithm[6].

An initial configuration was generated by randomly locating syndiotactic polystyrene (sPS) or atactic polystyrene (aPS) chains in a large simulation box (i.e., 0.1 g/cm3). In the case of aPS, aPS chains were generated with random sequences consisting of 50% right-handed and 50% left-handed monomers. Topological frustrations of the initial chain conformations were released by energy minimization with the steepest descent method, followed by a short NVT simulation. The initial velocities in the NVT simulation were randomly generated from Maxwell distribution. After the NVT simulation, NPT simulation was performed over 10 ns to equilibrate the system at 1 atm. The temperature and pressure were controlled by Nose-Hoover thermostat[7, 8] and Parrinello-Rahman barostat[9], respectively. The equilibrated system was used as an input for the production run of NVT simulation over 100 ns. Different temperatures were used in various simulations and 1 atm was used as the pressure in all simulations. The thermodynamic properties (e.g., the pressure tensor) were calculated at every 1 fs and the block-averaged at every 1 ps. The positions of all atoms were sampled at every 10 ps for calculating the mean squared displacement (MSD) and the chain conformations.

S.1.2 Coarse-Grained (CG) Simulations

We applied Iterative Boltzmann Inversion (IBI)[10] to derive the CG force fields, including the nonbonded, bond, angle, and dihedral potentials (see Figure S1 for example CG force fields for sPS). The distribution functions of nonbonded pairs, bond lengths, angles and dihedral angles obtained from the AA model with DP=20 were used as the reference for both sPS and aPS.

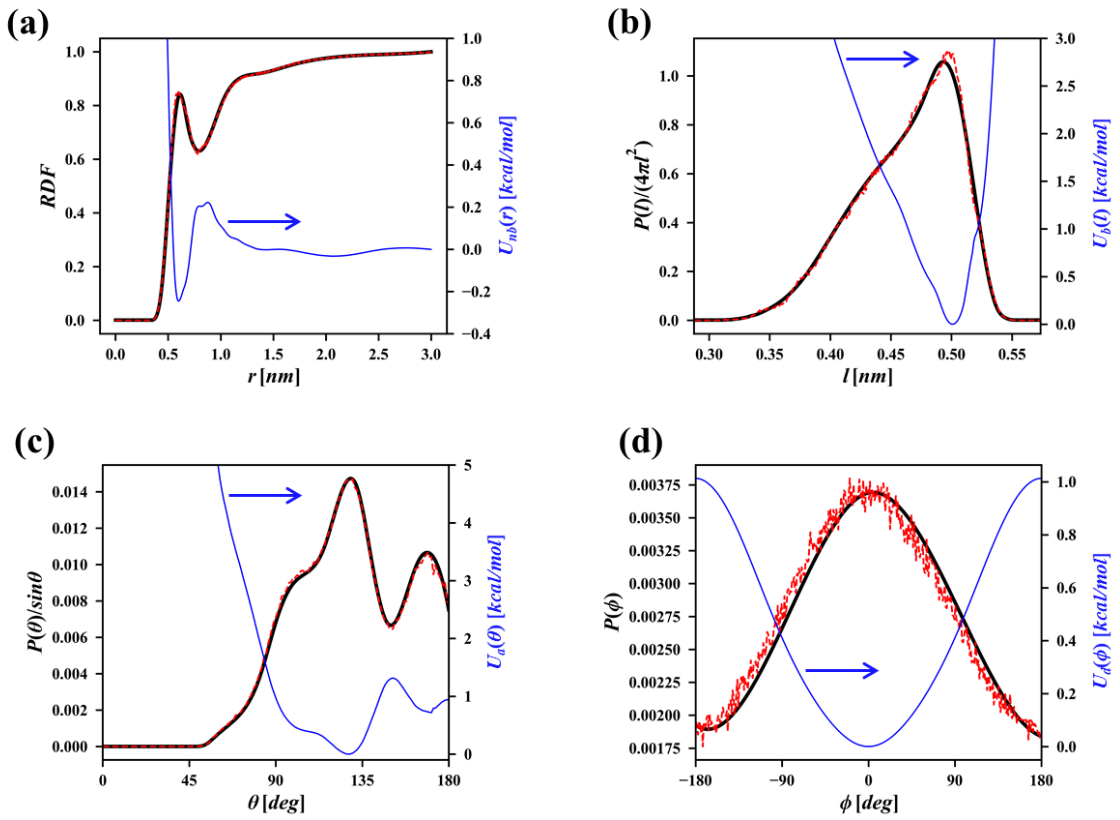

Figure S1. Examples of tabulated force fields (blue solid lines) developed for the coarse-grained (CG) model of syndiotactic polystyrene together with the distribution function obtained from the target all-atom (AA) model (black solid lines) and the CG model (red dashed lines). (a) Nonbonded pairwise potential and the radial distribution function (excluding 1-2, 1-3 and 1-4 bonded neighbors) of the (CG2, CG2) pair. (b) Bond potential and the bond length distribution function of the CG1-CG1 bond. (c) Angle potential and the bond angle distribution function of the CG2-CG1-CG2 angle. (d) Dihedral potential and the dihedral angle distribution of the CG1-CG1-CG1-CG1 dihedral.

We performed CG simulations of sPS and aPS melts with different degrees of polymerizations (DPs) from 20 to 600 using LAMMPS (version 7 Aug 2019)[11]. The initial configuration was generated by randomly adding sPS or aPS chains in a simulation box to achieve a designated density $\rho = 0.84$ g/cm^3. A soft-core potential $U_{soft}(r) = A_{soft}(1 + \cos(\pi r/r_c))$ with $r_c = 7$Å was applied to all CG beads. The energy of the soft-core potential A_{soft} was increased from 10 to 100 kcal/mol within 30 ps during an NVT simulation to push off CG beads

to avoid overlaps. Then the non-bonded pairwise potentials were switched back to the IBI-derived ones and a 3 ns NPT simulation was performed to relax the simulation box size. Finally, a relaxation run followed by a production run under the NVT ensemble was performed. The relaxation and production run lasts 20 ns and 100 ns for DP = 20~100, 100 ns and 400 ns for DP = 600. The temperature, 700 K, and pressure, 1 atm, of all CG simulations were controlled by the Nose-Hoover style thermostat and barostat[12], and the integration time step was set to 4 fs.

The root mean squared end-to-end distance of chains with different DPs is shown in Figure S2. At small DPs (DP < 100), the chain size increases faster than $\sqrt{\mathrm{DP}}$ due to the local rigidity of the sPS chain. At large DPs (DP ≥ 100), the chain size follows the ideal chain conformation, and $R_e = 0.788(\mathrm{DP})^{0.5}$ nm for sPS and $R_e = 0.657(\mathrm{DP})^{0.5}$ nm for aPS.

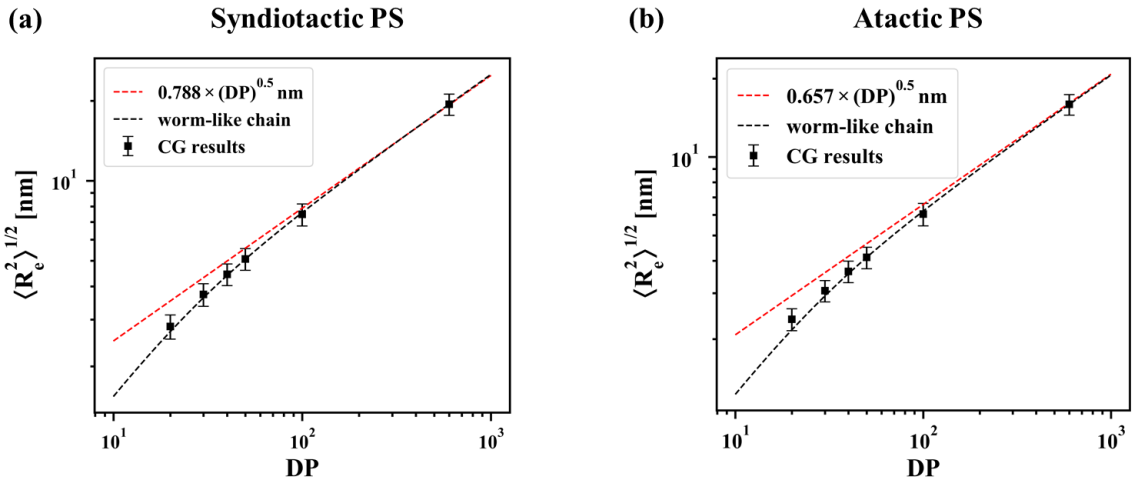

Figure S2. Root mean squared end-to-end distance of coarse-grained (CG) (a) syndiotactic polystyrene (sPS) and (b) atactic polystyrene (aPS) with different degree of polymerizations (DPs). The CG simulation data is shown as black squares and fitted with the worm-like chain model. At large DPs, the fitted worm-like chain model as well as the CG simulation data converge to the $0.788 \times (\mathrm{DP})^{0.5}$ nm for sPS and $R_e = 0.657(\mathrm{DP})^{0.5}$ nm for aPS, which agrees with the ideal chain conformation of polymers in a melt.

S.1.3 Slip-Spring (SS) Simulations

In the SS model, polymers are represented by a flexible chain of N_{ss} beads connected by harmonic springs. The bonded potential between two bonded beads *i* and *j* is described by

$$\beta U_{b,ij}(\boldsymbol{r}_{ij}) = \frac{3}{2}\boldsymbol{r}_{ij}^2/b^2 \tag{S1}$$

where $\beta = 1/(k_B T)$ and k_B is the Boltzmann constant, $\boldsymbol{r}_{ij}$ is the bond vector, *b* is the bond length. The nonbonded potential between beads *i* and *j* is described by

$$\beta U_{nb,ij}(\boldsymbol{r}_{ij}) = \frac{\sqrt{\bar{N}}}{R_e^3}\kappa N \times I(\boldsymbol{r}_{ij}) \tag{S2}$$

where $\bar{N} = (\rho_0 R_e^3/N)^2$ is the invariant degree of polymerization, where ρ_0 is the bead number density, R_e is the end-to-end distance of the polymer chain, N is the number of beads in each chain. κ is a parameter related to the inverse of compressibility. The function $I(\boldsymbol{r}_{ij})$ depends on the displacement vector between the two beads $\boldsymbol{r}_{ij} = \boldsymbol{r}_j - \boldsymbol{r}_i$ and is calculated as

$$I(\boldsymbol{r}_{ij}) = \int \mathrm{d}^3\boldsymbol{r}\, w(\boldsymbol{r} - \boldsymbol{r}_i) w(\boldsymbol{r} - \boldsymbol{r}_j) \tag{S3}$$

where $w(\boldsymbol{r})$ is the normalized density cloud so the $\rho_0 \int \mathrm{d}^3\boldsymbol{r}\, w(\boldsymbol{r}) = 1$. For simplicity, we choose a uniform density cloud

$$w(\boldsymbol{r}) = \begin{cases} 1, & |\boldsymbol{r}| \le 0.5 r_{cut} \\ 0, & |\boldsymbol{r}| > 0.5 r_{cut} \end{cases} \tag{S4}$$

where the cutoff distance $r_{cut} = (3n_i/4\pi\rho_0)^{1/3}$ is chosen by setting the mean number of interacting beads $n_i = 14$. The topological constraints are modeled by introducing slip-springs. A slip-spring is a "topological bond" connecting a pair of beads from different chains and introduces an extra interaction potential

$$\beta U_{ss,ij}(\boldsymbol{r}_{ij}) = \frac{3}{2}\boldsymbol{r}_{ij}^2/b_{ss}^2 \tag{S5}$$

where $\boldsymbol{r}_{ij}$ is the slip-spring bond vector, b_{ss} is the slip-spring bond length that determines its strength and is chosen to be $b_{ss} = b$. The slip-spring evolves by hopping from one bead to its neighboring beads and can be created/destroyed at the chain end, both in a Monte Carlo manner as described by Ramírez-Hernández *et al.*[13] With the abovementioned formulism for the system interaction potential, the force acting on each bead can be obtained by $\boldsymbol{f}_i = \boldsymbol{f}_i^b + \boldsymbol{f}_i^{nb} + \boldsymbol{f}_i^{ss} = -\nabla\left[U_{b,ij}(\boldsymbol{r}_{ij}) + U_{nb,ij}(\boldsymbol{r}_{ij}) + U_{ss,ij}(\boldsymbol{r}_{ij})\right]$. The system is updated by a hybrid scheme, where the position of beads are updated via Brownian dynamics and the slip-spring configurations are updated via Monte Carlo moves every τ_{ss} time units. Therefore, the equation of motion is integrated for each bead

$$m\gamma\boldsymbol{v}_i(t) = \left[\boldsymbol{f}_i^b + \boldsymbol{f}_i^{nb} + \boldsymbol{f}_i^{ss}\right] + \sqrt{2m\gamma k_B T}\boldsymbol{R}_i(t) \tag{S6}$$

where the mass of the bead m is set to unity, $\gamma = 1\tau^{-1}$ is the friction coefficient (τ is the time unit), the second term on the r.h.s of the equation is the random force where $\boldsymbol{R}_i(t)$ is a Gaussian process satisfying $\langle \boldsymbol{R}_i(t) \rangle = 0$ and $\langle \boldsymbol{R}_i(t) \boldsymbol{R}_j(t') \rangle = \delta_{ij}\delta(t - t')$. The quantities in the SS model are in reduced units. The chain size R_e sets the unit of length and the simulation box size is $(2R_e)^3$. The energy is measured in k_BT units. The simulation is performed for 3×10^6 steps with timestep $\Delta t = 0.0002\tau$. The hopping/creation/destruction of slip-springs are performed in each time step. The stress of the system is computed from the sum of the bonded, nonbonded, and slip-spring interactions.

To model a polymer melt, we need to determine the following parameters in the SS model: the number of beads per chain (N_{ss}), the bead number density (ρ_0), and the compressibility (κ). In our slip-spring simulations of sPS melts, we chose to discretize an entangled strand to $N_{e,ss} = 4$ slip-spring beads. Since the DP of an entangled strand is $N_e = 126$ as obtained from CG simulations using the Z1 algorithm[14-16], the number of beads per chain is $N_{ss} = \text{DP} \times N_{e,ss}/N_e$. From CG simulations, we also obtained the root mean squared end-to-end distance of a chain $R_e = 0.788(\text{DP})^{0.5}\ nm$ for $\text{DP} \geq 100$ (see Figure S2(a)), so the bead number density is $\rho_0 = \rho R_e^3 N_{e,ss} N_A/(M_0 N_e) = 0.0743(\text{DP})^{1.5}$, where $\rho = 0.827\ \text{g/cm}^3$ is the density, $M_0 = 104.15\ \text{g/mol}$ is the molecular weight of a monomer, and N_A is the Avogadro's number. The compressibility is chosen to be $\kappa = 3.58$. Similarly, in the slip-spring model of aPS melts, we chose to represent an entangled strand with $N_{e,ss} = 3$ beads. Since and the density of aPS is similar to that of sPS, The bead number density of aPS was determined by $\rho_0 = \rho R_e^3 N_{e,ss} N_A/(M_0 N_e) = 0.0226(\text{DP})^{1.5}$, where the root mean squared end-to-end distance of a chain is $R_e = 0.657(\text{DP})^{0.5}\ nm$ for $\text{DP} \geq 600$ (see Figure S2(b)), the DP of an entangled strand is $N_e = 180$ as obtained from CG simulations and the density is $\rho = 0.827\ \text{g/cm}^3$.

S.1.4 Building the Master Curve for Atactic Polystyrene

The master curves of aPS melts at 700K with DP $\gg N_e$ were obtained by combining the stress relaxation modulus from three models: (i) AA model with DP = 50, (ii) CG model with DP = 600, after rescaling the time and modulus by $\tau_{\text{CG-AA}} = 7.13$ and $\gamma_{\text{CG-AA}} = 1$, respectively, (iii) SS model with DP > 600, after rescaling the time and modulus by $\tau_{\text{SS-AA}} = \tau_{\text{SS-CG}} \times \tau_{\text{CG-AA}} = 1.43\times10^4$ ns and $\gamma_{\text{SS-AA}} = \gamma_{\text{SS-CG}} \times \gamma_{\text{CG-AA}} = 5\times10^5$ Pa, respectively. Figures S3(a) and S3(b) show the master curve, as well as the storage and loss moduli of aPS melts with DP = 600, 1200, 2100, and 2700,

where the latter is obtained from the Fourier transform of G(t) which is fitted with a generalized Maxwell model.

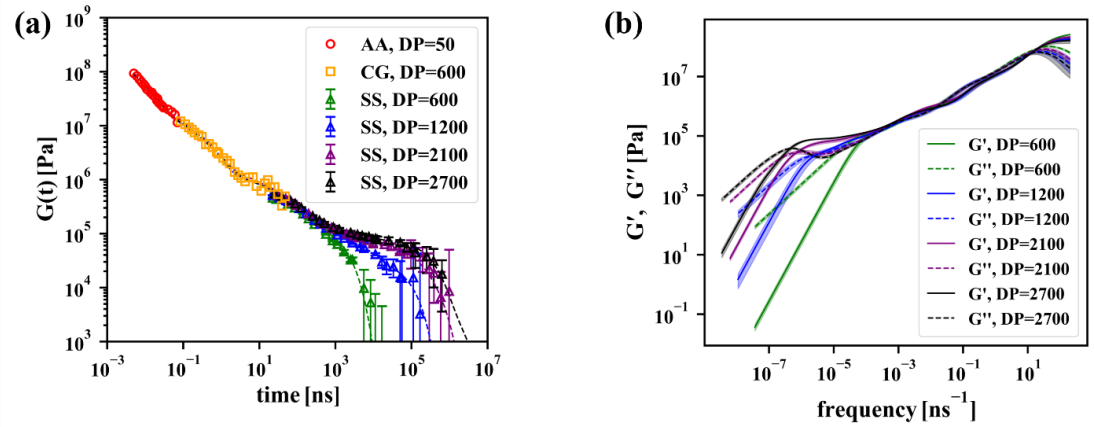

Figure S3. (a) Stress relaxation modulus master curves of entangled aPS melts at 700K built from all-atom (AA, red circles), coarse-grained (CG, orange squares) and slip-spring (SS, green, blue, purple, and black triangles) models. Error bars of the SS model indicate the uncertainty obtained from 6 parallel samples. Dashed lines are best fits of the master curve for aPS melt with DP = 600 (green), 1200 (blue), 2100 (purple), and 2700 (black) using generalized Maxwell model. (b) Storage (solid lines) and loss (dashed lines) moduli of aPS melt at 700K with DP = 600 (green), 1200 (blue), 1260 (purple), and 2700 (black). Shadows indicate the uncertainty obtained from 6 independent realizations of the simulation.

To extrapolate the viscoelastic properties measured at 700K to lower temperatures, we use the time-temperature superposition approach. AA simulations of aPS melts with DP = 50 are performed at various temperatures in the range T = 500~700 K. We then superimpose the stress relaxation modulus at a reference temperature T_0 = 500K using the time-shift factor a_T and the modulus-shift factor b_T as shown in Figure S4.

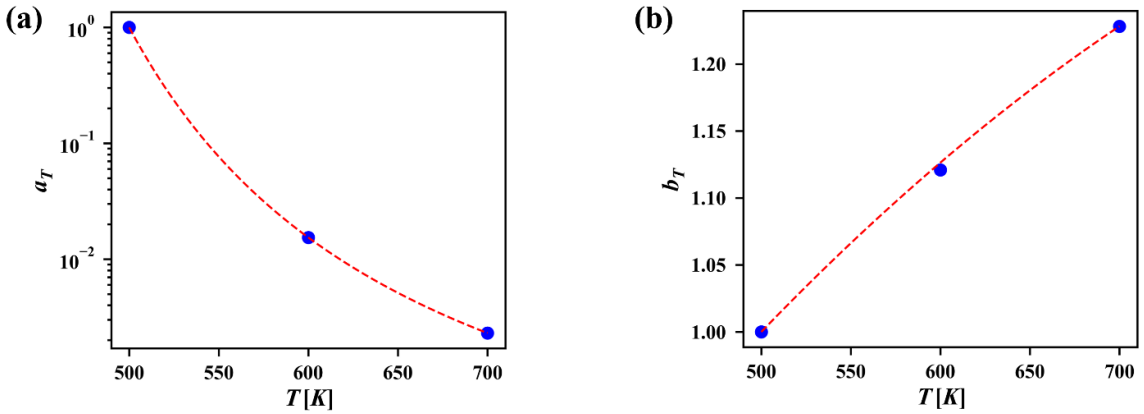

Figure S4. (a) Time-shift factor a_T of aPS as a function of temperature T. Red dashed line is the best fit of eq 2a in the main text with T_0 = 500 K. (b) Modulus-shift factor b_T of aPS as a function of temperature T. Red dashed line corresponds to eq 2b using $\rho(T)/(\mathrm{kg\cdot m^{-3}}) = 1240.5 - 0.5825 \times T/\mathrm{K}$, T_0 = 500 K and ρ_0 = 956.4 kg·m^{-3}.

S.2 Mean Squared Displacement of Syndiotactic Polystyrene Chain in Coarse-Grained and Slip-Spring Simulations

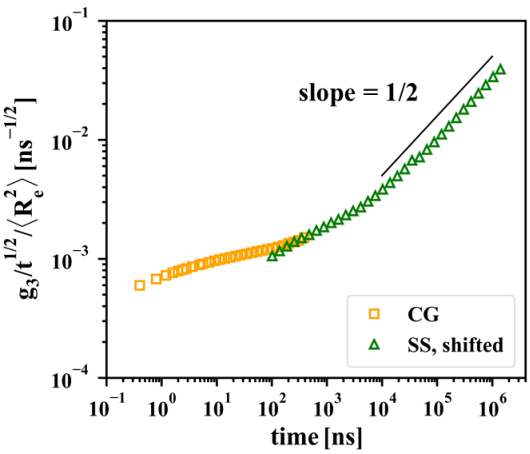

Figure S5. Mean squared displacement of chain, g_3, of the syndiotactic polystyrene melt with degree of polymerization DP = 600 in coarse-grained (CG) and slip-spring (SS) simulations. $\langle R_e^2 \rangle$ is the mean squared chain end-to-end distance. The 1/2 scaling at long time scales from the SS simulation indicates the diffusive behavior after disentanglement, i.e., $g_3 \sim t$. Since the melt is not strongly entangled (the number of entanglements per chain is $Z \approx 5$), the dynamics of this melt at shorter time scales is faster than the predicted scaling for highly entangled melts, $g_3 \sim t^{1/2}$. This is manifested by the almost flat but slowly increasing curve from ~1 to ~10^3 ns.

S.3 Monomer Mean Squared Displacement of Syndiotactic Polystyrene Melts with Different Degrees of Polymerization

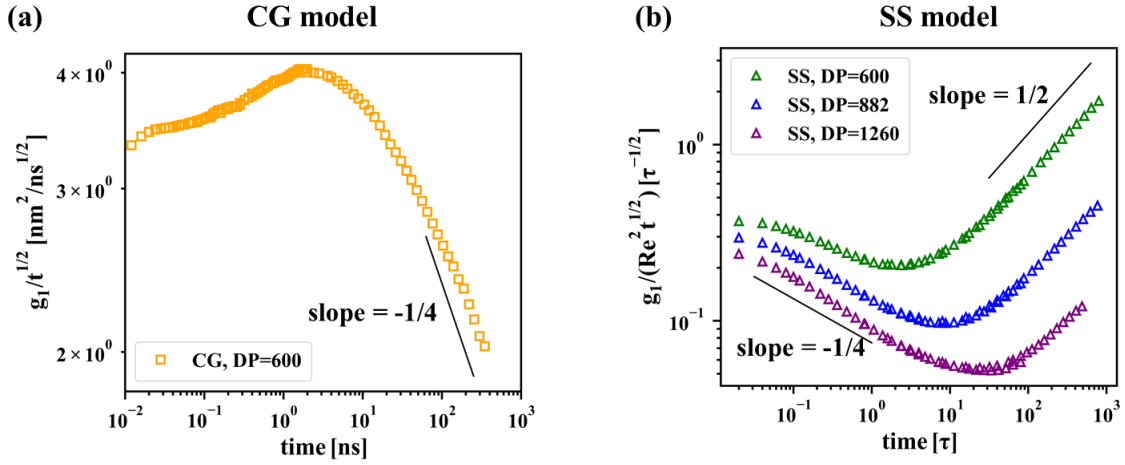

Figure S6. Monomer mean squared displacement, g_1, of syndiotactic polystyrene melts with different degrees of polymerizations (DPs) in (a) coarse-grained (CG) and (b) slip-spring (SS) simulations. The time and modulus of CG and SS results are not renormalized. The power law slope -1/4 in both CG and SS models indicates entanglement. The power law slope 1/2 in the SS model indicates diffusive behavior thus fully relaxed dynamics.

S.4 Stress Relaxation Modulus of Syndiotactic Polystyrene Melts with Different Degrees of Polymerization at Short Time Scales

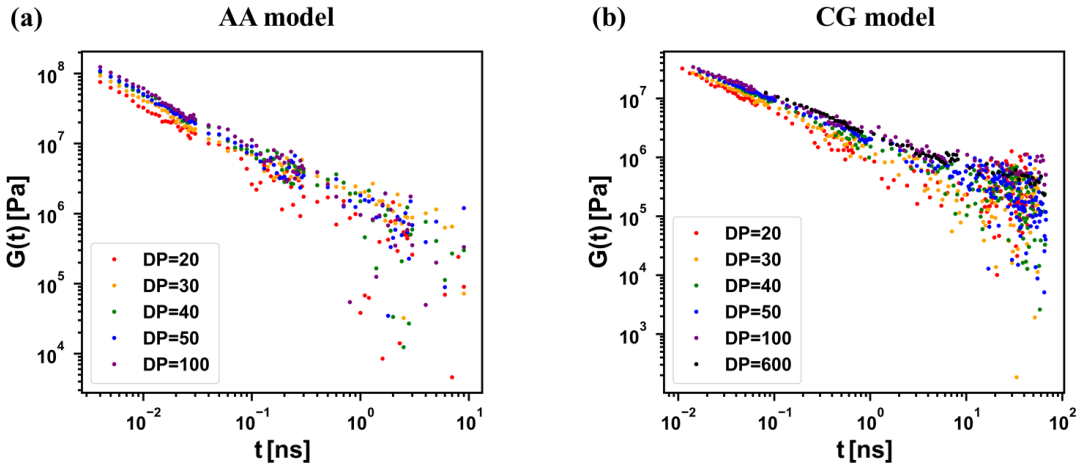

Figure S7. Stress relaxation modulus of syndiotactic polystyrene melts with different degrees of polymerizations (DPs) in (a) all-atom (AA) and (b) coarse-grained (CG) simulations. The time and modulus of CG results are not renormalized. At $t \leqslant 1$ ns, the stress relaxation modulus of the AA model converges at DP = 100. At $t \leqslant 10$ ns, the stress relaxation modulus of the CG model converges at DP = 600.

REFERENCES

1. Abraham, M. J. v. d. S., D.; Lindahl, E.; Hess, B; GROMACS development team. GROMACS User Manual version 5.1.4. www.gromacs.org
2. Berendsen, H. J.; van der Spoel, D.; van Drunen, R. GROMACS: a message-passing parallel molecular dynamics implementation. *Comput. Phys. Commun.* **1995,** 91 (1-3), 43-56.
3. van der Spoel, D.; Lindahl, E.; Hess, B.; Groenhof, G.; Mark, A. E.; Berendsen, H. J. GROMACS: fast, flexible, and free. *J. Comput. Chem.* **2005,** 26 (16), 1701-1718.
4. Jorgensen, W. L.; Maxwell, D. S.; Tirado-Rives, J. Development and testing of the OPLS all-atom force field on conformational energetics and properties of organic liquids. *J. Am. Chem. Soc.* **1996,** 118 (45), 11225-11236.
5. Ribeiro, A. A.; Horta, B. A.; Alencastro, R. B. d. MKTOP: a program for automatic construction of molecular topologies. *J. Braz. Chem. Soc.* **2008,** 19, 1433-1435.
6. Hess, B.; Bekker, H.; Berendsen, H. J.; Fraaije, J. G. LINCS: a linear constraint solver for molecular simulations. *J. Comput. Chem.* **1997,** 18 (12), 1463-1472.
7. Nosé, S. A unified formulation of the constant temperature molecular dynamics methods. *J. Chem. Phys.* **1984,** 81 (1), 511-519.
8. Hoover, W. G. Canonical dynamics: Equilibrium phase-space distributions. *Phys. Rev. A* **1985,** 31 (3), 1695.
9. Parrinello, M.; Rahman, A. Crystal structure and pair potentials: A molecular-dynamics study. *Phys. Rev. Lett.* **1980,** 45 (14), 1196.
10. Reith, D.; Pütz, M.; Müller-Plathe, F. Deriving effective mesoscale potentials from atomistic simulations. *J. Comput. Chem.* **2003,** 24 (13), 1624-1636.

11. Plimpton, S. Fast parallel algorithms for short-range molecular dynamics. *J. Comput. Phys.* **1995,** 117 (1), 1-19.
12. Shinoda, W.; Shiga, M.; Mikami, M. Rapid estimation of elastic constants by molecular dynamics simulation under constant stress. *Phys. Rev. B* **2004,** 69 (13), 134103.
13. Ramírez-Hernández, A.; Peters, B. L.; Andreev, M.; Schieber, J. D.; de Pablo, J. J. A multichain polymer slip-spring model with fluctuating number of entanglements for linear and nonlinear rheology. *J. Chem. Phys.* **2015,** 143 (24), 243147.
14. Kröger, M. Shortest multiple disconnected path for the analysis of entanglements in two- and three-dimensional polymeric systems. *Comput. Phys. Commun.* **2005,** 168 (3), 209-232.
15. Hoy, R. S.; Foteinopoulou, K.; Kröger, M. Topological analysis of polymeric melts: Chain-length effects and fast-converging estimators for entanglement length. *Phys. Rev. E* **2009,** 80 (3), 031803.
16. Karayiannis, N. C.; Kröger, M. Combined molecular algorithms for the generation, equilibration and topological analysis of entangled polymers: Methodology and performance. *Int. J. Mol. Sci.* **2009,** 10 (11), 5054-5089.